

The Physics of Protoplanetary Dust Agglomerates. III. Compaction in Multiple Collisions

René Weidling, Carsten Güttler, Jürgen Blum

*Institut für Geophysik und extraterrestrische Physik, Technische Universität zu Braunschweig,
Mendelssohnstr. 3, D-38106 Braunschweig, Germany*

c.guettler@tu-bs.de

Frithjof Brauer

Max-Planck-Institut für Astronomie, Königstuhl 17, D69117 Heidelberg, Germany

ABSTRACT

To study the evolution of protoplanetary dust aggregates, we performed experiments with up to 2600 collisions between single, highly-porous dust aggregates and a solid plate. The dust aggregates consisted of spherical SiO_2 grains with $1.5 \mu\text{m}$ diameter and had an initial volume filling factor (the volume fraction of material) of $\phi_0 = 0.15$. The aggregates were put onto a vibrating baseplate and, thus, performed multiple collisions with the plate at a mean velocity of 0.2 m s^{-1} . The dust aggregates were observed by a high-speed camera to measure their size which apparently decreased over time as a measure for their compaction. After 1000 collisions the volume filling factor was increased by a factor of two, while after ~ 2000 collisions it converged to an equilibrium of $\phi \approx 0.36$. In few experiments the aggregate fragmented, although the collision velocity was well below the canonical fragmentation threshold of $\sim 1 \text{ m s}^{-1}$. The compaction of the aggregate has an influence on the surface-to-mass ratio and thereby the dynamic behavior and relative velocities of dust aggregates in the protoplanetary nebula. Moreover, macroscopic material parameters, namely the tensile strength, shear strength, and compressive strength, are altered by the compaction of the aggregates, which has an influence on their further collisional behavior. The occurrence of fragmentation requires a reassessment of the fragmentation threshold velocity.

Subject headings: Solar Nebula, Planetesimals, Experimental Techniques, Collision Physics, Solar System Origin

1. Introduction

The formation of planets in the accretion disks around young stars starts with the growth of (sub-)micrometer-sized dust grains. Embedded in the thin gas of the disk, the dust grains collide due to a Brownian relative motion and inevitably stick at the small collision velocities (Blum et al. 2000; Krause and Blum 2004). By this mechanism, dust grains can grow to fractal aggregates of $\sim 100 \mu\text{m}$ before systematic drift significantly increases the collision velocities (Weidenschilling and Cuzzi 1993). Numerical simulations as well as

laboratory experiments have shown that for these increasing collision velocities, aggregates are restructured and grow to non-fractal but still very porous bodies (Dominik and Tielens 1997; Blum and Wurm 2000) so that growth can continue to larger sizes.

Once the aggregation has reached millimeter sizes, further growth due to sticking collisions between similar-sized dust aggregates slows down. Different experiments have shown that collisions of mm-sized aggregates result in bouncing or fragmentation: Blum and Münch (1993) performed

collision experiments with ZrSiO_4 dust aggregates with a volume filling factor (the fraction of volume filled with material) of $\phi = 0.26$. For velocities exceeding $\sim 1 \text{ m s}^{-1}$ they found fragmentation as the dominant process, whereas for smaller velocities the aggregates bounced. Heißelmann et al. (2007) performed similar experiments with highly porous aggregates ($\phi = 0.15$) of 1 – 5 mm diameter, which collided with a dusty target at a velocity of 0.2 m s^{-1} or with each other at 0.4 m s^{-1} . In both types of collisions the results were dominated by bouncing. Langkowski et al. (2008) [hereafter paper II], performed impact experiments of the same highly porous dust aggregates of 0.2 to 3 mm diameter and different materials onto equally porous targets of 25 mm diameter. For intermediate velocities (0.5 to 2.5 m s^{-1}) and projectile sizes (0.5 to 2 mm) they found bouncing of the aggregate which was even more likely if the target was "molded" to a non-flat surface (see Fig. 1c in paper II). Smaller projectiles and lower velocities led to sticking of the dust aggregate on the target surface, whereas larger projectiles and higher velocities resulted in a deep penetration of the projectiles with no possibility for escape (paper II). All those experiments were performed without the influence of gravity (free fall, drop tower or parabolic flight) and in all experiments the coefficient of restitution ε (the velocity after the impact divided by the velocity before impact) was rather small ($\varepsilon \lesssim 0.4$).

Many experiments of paper II and Heißelmann et al. (2007) were performed with the same sample material. While in paper II different compositions were used (SiO_2 (monodisperse spheres), irregular SiO_2 , and irregular diamond), Heißelmann et al. (2007) focussed on porous aggregates of $1.5 \mu\text{m}$ diameter SiO_2 monospheres. They were formed by the random ballistic deposition mechanism introduced by Blum and Schräpler (2004) and Blum et al. (2006) [hereafter paper I], had a diameter of 25 mm, and a volume filling factor of $\phi = 0.15$. The dust samples could be cut or broken into mm-sized aggregates to perform the collision experiments. Although pure silica is not the most abundant material in protoplanetary nebulae, paper I and II showed that the material properties of the dust (composition, size distribution, and shape) do not significantly alter the experimental outcome. Therefore, we regard the material repre-

sentative according to their mechanical properties of aggregates made of a broad collection of refractory grains and use the same material in the experiments presented below.

The motivation for this work is the explanation of the coefficient of restitution in the collisions of the described mm-sized SiO_2 aggregates, which is as low as $\varepsilon = 0.2$ in aggregate-aggregate as well as in aggregate-target collisions (Heißelmann et al. 2007). This means that only a few percent of the translational energy are conserved, whereas the bulk of energy is dissipated in an unknown manner. Although the aggregates of Heißelmann et al. (2007) do not show apparent deformation after the collisions, the obvious assumption is that the energy is consumed by compression. In a microscopic view, compression results from the rolling, breaking and restructuring of inter-grain contacts which dissipates energy (e.g. Paszun and Dominik 2008). In a macroscopic view, compression can be described by a compressive strength curve $p(\phi)$ (Blum and Schräpler 2004; Güttler et al. 2009, paper I). The dissipated energy in this context is $\Delta E = p \Delta V$, where ΔV is the decrease of a volume inside the dust aggregate with internal pressure p .

In this work, we describe an experiment, in which a dust aggregate with $\sim 2 \text{ mm}$ diameter is placed on a vibrating baseplate and is thus forced to perform multiple collisions with this plate. Although this is not a zero gravity experiment, gravity is not important for the individual collisions as Heißelmann et al. (2007) have shown that even under microgravity conditions sticking never occurs at the relevant velocities of $\sim 0.2 \text{ m s}^{-1}$ and that the collision time is too short for substantial gravitational influence (see the image sequence in Figs. 4 and 5 of Heißelmann et al. (2007)). The velocities are the same as those between aggregate and target in the experiments of Heißelmann et al. (2007). Performing multiple collisions, the cumulative compaction is larger than in a single collision and can, thus, be assessed.

In section 2 we describe the experimental setup for the measurement of the aggregate compaction in multiple collisions. The results are presented in section 3 and the relevance and consequences for dust aggregates in the protoplanetary nebula are discussed in section 4.

2. Experimental Setup

As a starting material for a mm-sized, highly porous protoplanetary dust aggregate we chose the well-defined dust aggregates introduced and characterized by Blum and Schr apler (2004). They consist of $1.5 \mu\text{m}$ diameter monodisperse SiO_2 spheres, possess a volume filling factor of $\phi_0 = 0.15$ and were formed by random ballistic deposition (Blum and Schr apler 2004). From these 25 mm aggregates we cut out cubes of ~ 2.5 mm diameter with a compaction of the aggregate rim to a maximum of $\phi = 0.16$ (Hei elmann et al. 2007). Each small aggregate was weighed (mass

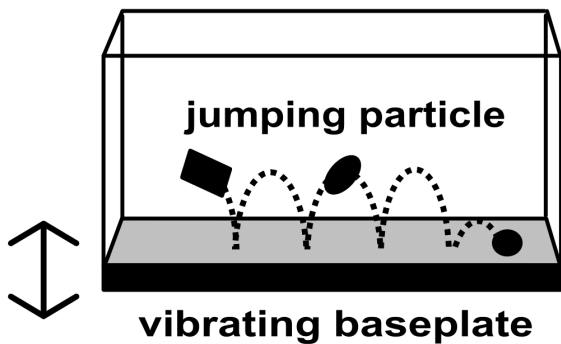


Fig. 1.— Experimental setup: The dust aggregate in the box is continuously colliding with the vibrating baseplate, while it is observed by a high-speed camera. The aluminum baseplate vibrates with a frequency of 100 Hz with a peak-to-peak amplitude of 0.4 mm.

m_0) and put into a box with plexiglass walls and an aluminum baseplate of $40 \times 40 \text{ mm}^2$ size (Fig. 1). The aggregate was observed with a high-speed camera at a frame rate of 380 frames per second in back-light illumination while the box was vibrated in the vertical direction at a frequency of 100 Hz with a peak-to-peak amplitude of 0.4 mm for different durations (10 to 80 s). This led to a jumping motion of the aggregate and 200 to 2600 bouncing collisions, after which the aggregate (final mass m_{end}) and the eroded material in the box (total mass of the debris m_{er}) were again weighed.

In each image, the cross-sectional area and the position of the aggregate were measured. The position measurements yield the number of collisions, which are underestimated by $\sim 20 \%$, because collisions near the edge of the box were not illumi-

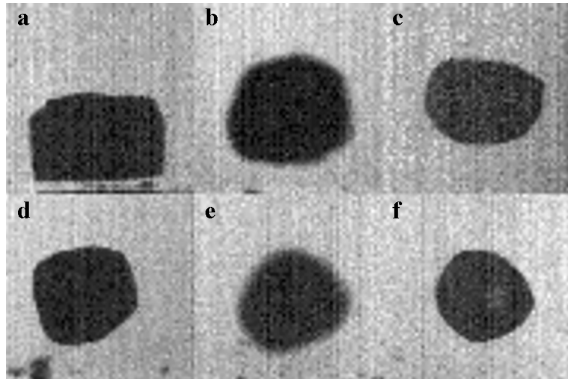


Fig. 2.— Sequence of a bouncing aggregate with ~ 150 collisions between two successive images. The aggregate is rounded first and is then clearly getting smaller. The width of the single frames is 4.6 mm. The example is taken from experiment 1 in Table 1.

nated well. From the maximum height between two collisions the aggregate’s velocity at the time of the collision can be determined assuming a free fall motion of the aggregate. Although the experiments were performed in air, the frictional effect of the ambient gas is negligible, as the maximum friction force $F_{\text{air}} = 6\pi\eta Rv = 9.5 \cdot 10^{-8} \text{ N}$ is much smaller than the projectile’s weight $F_{\text{grav}} = mg = 3.9 \cdot 10^{-5} \text{ N}$. Here m , R , v , and η are a typical aggregate mass ($m \approx 4 \text{ mg}$), the corresponding aggregate size ($R \approx 1.5 \text{ mm}$), an average aggregate velocity ($v \approx 0.2 \text{ m s}^{-1}$), and the viscosity of air ($\eta = 17.2 \mu\text{Pa s}$); g is the gravitational acceleration.

As the velocity of the baseplate is unknown for the exact time of collision, a statistical collision velocity distribution is presented in section 3. The imaged cross-sectional area of the aggregate was converted into a volume by assuming a sphere which is a coarse approximation at the onset of the experiments but a good approximation after ~ 150 collisions (Fig. 2). A total of 18 individual bouncing experiments was performed (Table 1).

3. Results

In this section, we present the calculation of the distribution of collision velocities. We will then quantify the compaction of the dust aggregates and give an analytical approximation for practi-

Table 1: Experimental results for all performed experiments. In the experiments marked with ^a the aggregate fragmented shortly after the given number of collisions.

experiment	initial mass m_0 [mg]	duration [s]	number of collisions	eroded mass [% of m_0]	mean collision velocity v [$\frac{\text{m}}{\text{s}}$]	resulting filling factor ϕ_{end}
1 ^a	4.96	71	2400	20	$0.213^{+0.042}_{-0.055}$	0.50
2	3.62	33	1200	9	$0.191^{+0.039}_{-0.055}$	0.32
3	3.90	43	1400	0	$0.199^{+0.042}_{-0.055}$	0.38
4	2.68	30	1050	34	$0.189^{+0.042}_{-0.055}$	0.25
5	2.64	13	550	9	$0.186^{+0.035}_{-0.052}$	0.28
6	2.88	14	250	12	$0.181^{+0.035}_{-0.049}$	0.21
7	2.10	10	200	24	$0.189^{+0.029}_{-0.047}$	0.16
8	2.34	15	500	-9	$0.186^{+0.037}_{-0.052}$	0.24
9	1.92	14	550	23	$0.206^{+0.039}_{-0.052}$	0.21
10	3.46	12	300	10	$0.189^{+0.035}_{-0.047}$	0.21
11	4.46	46	1750	6	$0.194^{+0.045}_{-0.052}$	0.39
12	4.40	57	2150	13	$0.191^{+0.039}_{-0.057}$	0.35
13	4.04	43	1650	8	$0.196^{+0.042}_{-0.057}$	0.32
14	4.60	77	2600	19	$0.201^{+0.039}_{-0.057}$	0.32
15 ^a	5.86	47	1700	14	$0.189^{+0.037}_{-0.055}$	0.34
16 ^a	3.86	17	500	7	$0.164^{+0.037}_{-0.057}$	0.23
17 ^a	4.44	53	2300	10	$0.199^{+0.042}_{-0.057}$	0.32
18	4.88	44	1600	8	$0.199^{+0.042}_{-0.052}$	0.34

cal use. Moreover, we will present further consequences of the structural change of the aggregates, namely the fragmentation of a dust aggregate at small velocities and the development of the coefficient of restitution.

3.1. Collision Velocities

The maximum height h of the dust aggregate between two collisions can be measured from the image with the highest aggregate position and it determines the aggregate's velocity at the time of impact, $v = \sqrt{2gh}$. As the impact time is only known with an error of 2.6 ms, as the maximum plate velocity of 0.13 m s^{-1} is in the same range as the collision velocity, and as the baseplate velocity rapidly changes, we make a statistical approach to calculate the distribution of collision velocities. The probability of a given plate velocity is given as

$$P(v) dv = \nu \cdot (t(v) - t(v + dv)), \quad (1)$$

where $\nu = 100 \text{ Hz}$ is the oscillation frequency of the plate and dv determines a velocity interval

around v . $t(v)$ is the inverse velocity cosine function

$$t(v) = \frac{1}{\omega} \arccos\left(\frac{v}{A_0\omega}\right), \quad (2)$$

where $A_0 = 0.2 \text{ mm}$ is the amplitude of the plate and $\omega = 2\pi\nu$ is the angular frequency. For an aggregate with velocity v_{ag} , plate velocities $v < -v_{\text{ag}}$ do not lead to a collision while the maximum plate velocity v_{pl} is the likeliest. Thus, the velocity distribution of the plate (Eq. 1) is convolved with a linear collision probability, cropped for $v < -v_{\text{ag}}$ and shifted by v_{ag} . This is the velocity distribution of a single collision. The same procedure is performed for each collision and all normalized distributions summed up yield the overall velocity distribution for one experiment. Figure 3 shows the mean of the velocity distributions of all experiments (solid line) with the standard deviation (grey shaded area). All velocities are smaller than 0.35 m s^{-1} , the median velocity is 0.19 m s^{-1} , while 50 % of all collisions are within 0.14 and 0.23 m s^{-1} . The velocity range for the individual experiments given in Table 1 is the 50 % range

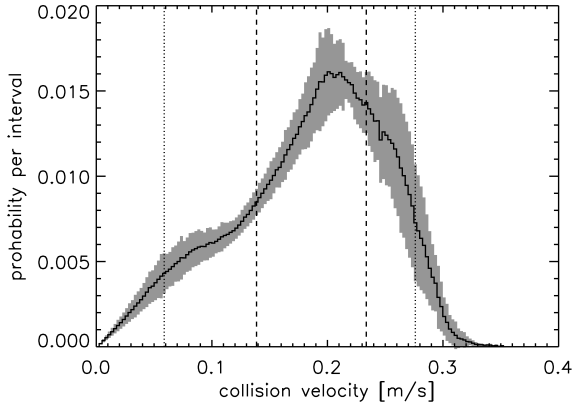


Fig. 3.— The mean of the impact velocity probabilities of all experiments (solid line) and the standard deviation from this distribution (grey shaded area). 50 % of the collision velocities are between the dashed lines, 90 % are between the dotted lines.

from the individual distributions.

3.2. Compaction of the Dust Aggregate

The prime objective of the experiments is to measure the increase of the averaged volume filling factor of the dust aggregate after n collisions, i.e.

$$\phi(n) = \phi_0 \cdot \frac{m(n)}{m_0} \cdot \frac{V_0}{V(n)}. \quad (3)$$

Here, m_0 is the initial mass of the aggregate, and V_0 is the initial volume calculated from m_0 by assuming an initial volume filling factor of $\phi_0 = 0.15$ (Blum and Schr apler 2004). The volume $V(n)$ was calculated from the projectile's cross section $\sigma_a(n)$ by assuming a sphere, thus, $V(n) = \frac{4}{3}\pi^{-1/2}\sigma_a(n)^{3/2}$. The mass $m(n)$ slightly decreases due to erosion at the target. However, experiments with different durations did not show any change in the relative erosion (see Table 1) and most of the eroded fragments were sticking to the baseplate at the place of the first few collisions. Thus, assuming that the erosion took place in the very first collisions and was caused by the preparation of the sample, we take $m(n) = m_{\text{end}}$.

The decrease of the volume of the dust aggregate over the course of collisions with the baseplate is obvious as presented in the image sequence of Fig. 2. From each experiment we calculated the volume filling factor $\phi(n)$ from Eq. 3 and

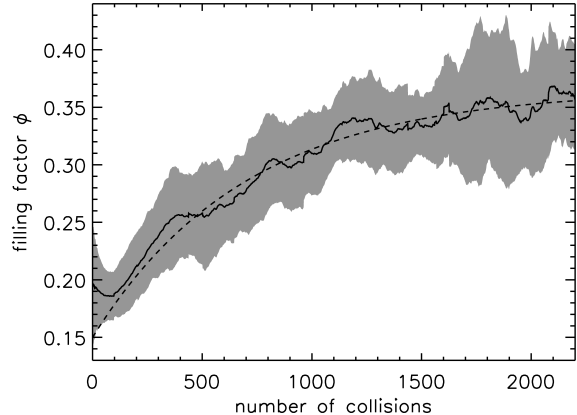


Fig. 4.— Mean increase of the volume filling factor from 18 individual experiments (solid line) and the standard deviation (grey shaded area). The dashed line represents an analytic approximation (Eq. 4) which converges to a filling factor of $\phi = 0.37$. The deviation for small collision numbers is determined by systematic errors in the experiments while the analytic curve is constrained to $\phi(n = 0) = \phi_0$.

took a boxcar average over 100 collisions to reduce stochastic scattering from the rotation of the aggregate. The mean filling factor and the standard deviation of all experiments are presented in Fig. 4 (solid line and grey shaded area).

The filling factor for $n < 150$ is greater than the initial filling factor of $\phi_0 = 0.15$, which is due to a combination of various systematic errors: The scaling is inaccurate if the aggregate is in the front or back of the box which results in an error of $\pm 3\%$ in ϕ , and the choice of the threshold for estimating the size yields an error of ${}^{+5}_{-0}\%$. In three experiments, the aggregate appeared from the smallest side in the beginning which overestimates ϕ , and the assumption of a sphere instead of the cuboid underestimates the filling factor until the aggregate is significantly rounded. Due to those uncertainties it is reasonable to regard the data only for $n > 150$ and assume $\phi(n = 0) = \phi_0$.

We give an analytic approximation which represents the filling factor for $n > 150$ (dashed line, Fig. 4):

$$\phi(n) = \phi_{\text{max}} - \Delta\phi \cdot e^{-n/\nu} \quad (4)$$

with $\phi_{\text{max}} = 0.365$, $\Delta\phi = \phi_{\text{max}} - \phi_0$ and $\nu = 700$. Accounting for the systematic error in the

collision number n , which is underestimated by 20 % (section 2), we take $\nu = 850$ for practical use. For later application, we can calculate the volume of the aggregate (from Eqs. 3 and 4) as a function of the collision number

$$V(n) = \frac{\phi_0 \cdot V_0}{\phi_{\max} - \Delta\phi \cdot e^{-n/\nu}}, \quad (5)$$

where we ignore the mass loss in the first collisions and take $m(n) = m_0$.

In a very simple model, we assume that the compression is the cause for the loss of kinetic energy, thus

$$(1 - \varepsilon^2) \cdot \frac{1}{2} \cdot m \cdot v^2 = p \cdot \Delta V, \quad (6)$$

where ΔV for the first collision can be calculated by deriving Eq. 5 for $n = 0$ and $\Delta n = 1$:

$$\Delta V = \frac{V_0 \cdot \Delta\phi}{\phi_0 \cdot \nu}. \quad (7)$$

Thus, we can calculate the pressure in the aggregate (first collision) as

$$p = \frac{(1 - \varepsilon^2) \cdot m \cdot v^2 \cdot \phi_0 \cdot \nu}{2 \cdot V_0 \cdot (\phi_{\max} - \phi_0)}. \quad (8)$$

For an aggregate with $m = 4.24$ mg, $V_0 = 14.1$ mm³, $v = 0.2$ m s⁻¹, and $\varepsilon = 0.2$ this yields a pressure of 3424 Pa. Using the compressive strength curve proposed by Güttler et al. (2009) we can calculate the volume filling factor ϕ_c in the compressed volume ΔV_c to be

$$\phi_c(p) = \phi_2 - \frac{\phi_2 - \phi_1}{\exp\left(\frac{\lg p - \lg p_m}{\Delta}\right) + 1}. \quad (9)$$

For omnidirectional dynamic compression, Güttler et al. (2009) developed the empirical parameters $\phi_1 = 0.12$, $\phi_2 = 0.58$, $\Delta = 0.58$, and $p_m = 1300$ Pa, which yields a volume filling factor $\phi_c = 0.43$, which is slightly higher than the end compression $\phi_{\max} = 0.365$ of the aggregate.

The relation between the volume decrease of the agglomerate ΔV and the volume ΔV_c with compressed material is determined by the mass balance in the volume ($\Delta V + \Delta V_c$):

$$\frac{\Delta V_c}{\Delta V} = \frac{\phi_0}{\phi_c - \phi_0} \quad (10)$$

If we assume that this relation holds for every collision, we can calculate the volume fraction of the compressed material for the equilibrium situation $n \rightarrow \infty$ to be:

$$f_c = \frac{\int \Delta V_c \, dn}{V(n \rightarrow \infty)} \quad (11)$$

$$= \frac{\frac{\phi_0}{\phi_c - \phi_0} \cdot \int \Delta V \, dn}{\frac{\phi_0}{\phi_{\max}} \cdot V_0} \quad (12)$$

$$= \frac{\phi_{\max}}{\phi_c - \phi_0} \cdot \frac{V_0 - V(n \rightarrow \infty)}{V_0} \quad (13)$$

$$= \frac{\phi_{\max} - \phi_0}{\phi_c - \phi_0} \quad (14)$$

Inserting the given values, we learn that the volume of the compressed material for $n \rightarrow \infty$ is 77 % of the end volume of the agglomerate. Thus, the aggregate is inhomogeneously compacted and has an unaltered core of 61 % in radius.

3.3. Influence of the Compaction on the Mechanical Properties

The change of the volume filling factor must clearly have an influence on the mechanical properties of the dust aggregate. One related finding is that in four experiments the aggregate fragmented during the succession of impacts (Fig. 5). Those experiments are marked in Table 1 and do not show a clear systematic difference to the other experiments in which the aggregate did not fragment. The number of collisions and the filling factors in those experiments are rather high – except for experiment 16. A possible explanation is a de-

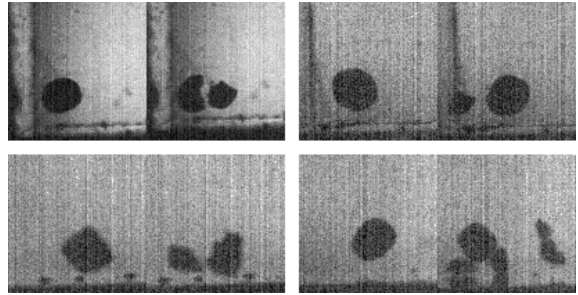


Fig. 5.— The four cases in which the aggregate fragmented (from The fragmentation is rather gentle, such that the aggregates only break into few. The width of a single frame is 7.7 mm.

crease of the critical fragmentation velocity with

increasing volume filling factor or, at least, an increasing breakup probability. Figure 5 shows very gentle fragmentation in contrast to the broad size distribution of fragments found at higher velocities (Blum and Münch 1993). This breakup is usually found when fragmentation occurs at velocities near the fragmentation threshold. However, as the dependence on the number of collisions does not show a clear tendency, a second explanation is a general breakup probability for which we can give a rough estimate for mm-sized dust aggregates in low-velocity collisions as:

$$P_{\text{frag}} = \frac{4 \pm 2}{\sum n_{\text{coll}}} = (1.8 \pm 0.9) \cdot 10^{-4} \text{ per collision}, \quad (15)$$

where $\sum n_{\text{coll}} = 22650$ is the total number of collisions in all experiments (Table 1).

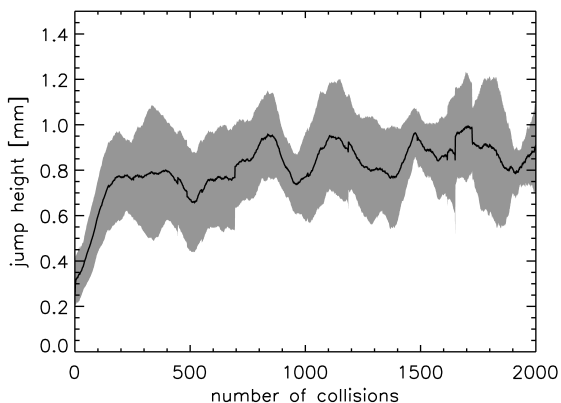


Fig. 6.— The jump height of the aggregate (mean of all experiments) over the number of collisions. The averaging was taken for as many experiments as possible: While for the first collisions all experiments could be utilized, for collision numbers of more than 2000 only few experiments were available. For $n > 150$ the jump height only slightly increases with the number of collisions (also meaning compactness), which unexpectedly indicates a constant coefficient of restitution.

Another influence of the structural change might be expected for the coefficient of restitution: The coefficient of restitution is a measure for the dissipation of energy and from section 3.2 we know that compaction is a plausible dissipation mechanism. However, as the compaction is not constant over time, the coefficient of restitution is not expected to be either. As the mean

baseplate velocity does not change with time, a change in the coefficient of restitution would result in a variation of the maximum height of the aggregate. Figure 6 shows that the jump height of the aggregate does only slightly increase with time for $n > 150$. A linear fit of all heights for $200 < n < 2000$ yields a mean slope of $40 \mu\text{m} / 1000$ collisions. The increasing height in the very beginning might be due to structural changes but concurrently the aggregate always collides with a broad side in these first collisions, which must have a substantial but unknown influence on the height.

4. Discussion

In this section we discuss the relevance for the protoplanetary nebula, namely, scaling the results for different sizes and velocities and estimating whether multiple bouncing collisions can occur in a reasonable timescale. Furthermore, we discuss the consequences of the aggregate compaction for their further evolution.

4.1. Collision Model

We will develop a scaling relation for the aggregate compaction in size and collision velocity. From the momentum balance of the colliding aggregate, we can give the pressure in the aggregate as

$$p = \frac{(1 + \varepsilon) \cdot m \cdot v}{\tau \cdot A} \quad (16)$$

$$= \frac{(1 + \varepsilon) \cdot m \cdot v \cdot \nu}{\tau \cdot 4 \cdot \pi \cdot R^2}, \quad (17)$$

where $(1 + \varepsilon) \cdot m \cdot v$ is the change of momentum of the colliding aggregate, taking place within the collision time τ , and A is the contact area with the baseplate. For the contact area we make the assumption that the total surface of the aggregate interacted after ν collisions ($A = 4\pi R^2/\nu$), where ν is the e-folding width of the exponential function in Eq. 4. Indeed, this simple model of maximum compaction of a $1/\nu$ fraction of the aggregate volume only if a previously passive site on the aggregate surface is hit, yields the very same behavior as Eq. 4, which justifies this assumption (see Fig. 7). Thus, we can combine Eqs. 8 and 17 to calculate the contact time

$$\tau = \frac{V_0 \cdot \Delta\phi}{(1 - \varepsilon) \cdot v \cdot \phi_0 \cdot 2 \cdot \pi \cdot R^2}. \quad (18)$$

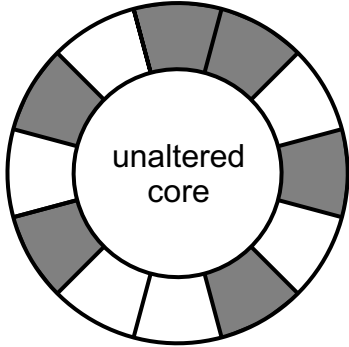


Fig. 7.— A simple 2D sketch of the compacted aggregate after some collisions. According to Eq. 14, 39 % of the aggregate radius are compacted around an unaltered core. The compacted rim is only compressed at the sites where the aggregate collided (grey volumes), and a second collision at the same site does not lead to further compaction. This simple model is capable to explain the increase of the volume filling factor according to Eq. 4.

For the parameters of the $R = 1.5$ mm aggregate in section 3.2 this leads to a contact time of $\tau = 8.9$ ms, which is a realistic result. Indeed, the collision time in the experiments of Heißelmann et al. (2007) can be confined to less than 20 ms (see their image sequence) and preliminary studies dedicated to measure the collision time of aggregates with $\phi \approx 0.35$ with a solid plate yield approximately 5 ms (Heißelmann et al., pers. comm.).

We approximate the situation by an elastic sphere with a Poisson number of zero, colliding with a wall and take the relation for the contact time from Hertz (1881) as

$$\tau = 3.85 \cdot \sqrt[5]{\frac{m^2}{v \cdot R \cdot G^2}}, \quad (19)$$

where G is the shear modulus of the sphere. Dintwa et al. (2008) compile the assumptions made in the Hertz model and value the importance of frictional contact, non-flat contact surface and large strains. As for the aimed accuracy in our model, the deviations from the Hertz model they found (and only for large strains) are rather small (within a few percent) so that we use Eq. 19 to calculate the shear modulus of the dust aggregate

to be $G = 944$ Pa. Combining Eqs. 18 and 19, we get a scaling relation for the compression of an aggregate as

$$\begin{aligned} \Delta\phi_{\text{sc}} &= \frac{24.2 \cdot (1 - \varepsilon) \cdot v \cdot \phi_0 \cdot R^2}{V_0} \cdot \sqrt[5]{\frac{m^2}{v \cdot R \cdot G^2}} \\ &\propto R^0 \cdot v^{4/5} \end{aligned} \quad (20)$$

The upper velocity limit for this extrapolation is 0.56 m s^{-1} as for this velocity the volume filling factor $\phi_{\text{max}} = \Delta\phi_{\text{sc}} + \phi_0$ reaches the physical maximum of $\phi_{\text{RCP}} \simeq 0.64$, which is the random close packing of spheres. This high filling factor is, however, unlikely to be reached in collisional compression, because the aggregate will then rather fragment. Thus, the model predicts a fragmentation threshold for $\sim 0.5 \text{ m s}^{-1}$ in multiple collisions. Velocities below a few mm s^{-1} lead to an insignificant compaction of $\Delta\phi_{\text{sc}} \lesssim 0.01$.

We follow the same Hertzian ansatz to derive a scaling relation for the the e-folding collision number $\nu_{\text{sc}} = 4\pi R^2/A$. The radius of the contact area A in the Hertz model is

$$a_0 = 0.86 \cdot \sqrt[5]{\frac{mR^2v^2}{\sqrt{G}}}. \quad (22)$$

Thus, the the e-folding collision number ν_{sc} scales like

$$\begin{aligned} \nu_{\text{sc}} &= 5.42 \cdot \sqrt[5]{\frac{GR^6}{m^2v^4}} \\ &\propto R^0 \cdot v^{-4/5} \end{aligned} \quad (23)$$

With the scaling relations in Eqs. 21 and 24 we get $\Delta\phi_{\text{sc}} = \Delta\phi \cdot \left(\frac{v}{0.2\text{m/s}}\right)^{4/5}$ and $\nu_{\text{sc}} = \nu \cdot \left(\frac{v}{0.2\text{m/s}}\right)^{-4/5}$ and we are able to give the increase of the aggregate's volume filling factor in each collision as

$$\phi^+(\phi) = \frac{\phi_0 + \Delta\phi \cdot \left(\frac{v}{0.2\text{m/s}}\right)^{4/5} - \phi}{\nu \cdot \left(\frac{v}{0.2\text{m/s}}\right)^{-4/5}} \quad (25)$$

with $\phi_0 = 0.15$, $\Delta\phi = 0.215$, and $\nu = 850$ for $v \lesssim 0.5 \text{ m s}^{-1}$. For a constant velocity this description is equivalent to Eq. 4 but it has the advantage that it is independent of the collision history of an aggregate (e.g. independent of n) and is therefore capable to account for non-constant bouncing velocities.

Table 2: The calculation of collision timescales τ_c for different solar-nebula models. For all models we use $\rho_d = 300 \text{ kg m}^{-3}$, $a = 1 \text{ AU}$, $T_0 = 280 \text{ K}$, $M_\star = M_\odot$, and $\alpha = 10^{-5}$.

solar-nebula model	$\Sigma_0 \text{ [g cm}^{-2}\text{]}$	δ	$R \text{ [mm]}$	$n \text{ [m}^{-3}\text{]}$	$v \text{ [cm s}^{-1}\text{]}$	$\tau_c \text{ [years]}$	$\tau_c \cdot \nu \text{ [years]}$
Weidenschilling (1977)	1700	1.50	1.50	$2.57 \cdot 10^{-1}$	0.27	1.62	1374
			2.66	$6.13 \cdot 10^{-2}$	20.00	0.03	24
Andrews and Williams (2007)	20	0.80	1.50	$2.79 \cdot 10^{-2}$	40.20	0.10	85
			0.11	$1.79 \cdot 10^1$	20.00	0.06	46
Desch (2007)	50500	2.17	1.50	1.40	0.02	4.00	3398
			77.50	$7.29 \cdot 10^{-5}$	20.00	0.03	24

4.2. Collision Timescale

To value the importance of the bouncing and compacting collisions, we estimate the timescale on which subsequent collisions occur in the protoplanetary nebula. For simplicity we make the best-case assumption that the entire mass is in the relevant aggregate size. A comparable sharp size distribution was found for the first growth of fractal aggregates (Krause and Blum 2004) but is unknown for the mm-size range. The mean collision timescale is then

$$\tau_c = \frac{1}{nv\sigma}, \quad (26)$$

where n is the number density of dust aggregates, $\sigma = 4\pi R^2$ is the collisional cross-section of two colliding aggregates, and v is the relative velocity. A broad size distribution does not extremely alter the effect of collisional compaction. If we consider such a wide size distribution and concentrate on the compaction of an aggregate at the high-mass end by collisions with smaller aggregates, the collision timescale decreases due to the increasing number density of smaller particles, $n \propto m^{-1}$, whereas the collision cross section and the relative velocity do not significantly change (see Fig. 8). The decrease in collision time is (partly) compensated by the smaller contact area in the collision (see Eq. 22) so that the number of collisions required to cover the whole surface of the large aggregate scales like $\nu \propto m^{-2/3}$. Thus, the relevant timescale for the total compaction scales as $\propto m^{1/3}$. Therefore the data given in Table 2 are upper limits. If we assume a gas-to-dust ratio of 100, we can give a general number density of dust aggregates in the midplane of the protoplanetary disk as

$$n = 1.88 \cdot 10^{-3} \frac{\Sigma_0}{\rho_d R^3} a^{\frac{\epsilon-3}{2}-\delta} \sqrt{\frac{M_\star}{T_0} \left(1 + \frac{R\rho_d a^\delta}{4\Sigma_0\alpha}\right)} \text{ m}^{-3}. \quad (27)$$

This equation follows directly from the expressions for the dust particle density in the midplane, Eqs. A16 and A18 in Brauer et al. (2007). Here, Σ_0 is the surface density of the gas in units of $[\text{g cm}^{-2}]$ at 1 AU in the disk, a is the distance to the star in [AU], δ and ϵ are the power indices for the surface density and temperature, respectively, M_\star is the mass of the star in $[M_\odot]$, T_0 is the temperature at 1 AU in units of [280 K], and R and ρ_d are the radius in [mm] and mass density in $[\text{kg m}^{-3}]$ of a representative dust aggregate. We assume that the dust particles are always in equilibrium between vertical dust settling towards the midplane of the disk and turbulent diffusion which mixes the dust up again into the higher regions of the protoplanetary disk (Dubrulle et al. 1995; Cuzzi and Weidenschilling 2006). Larger particles settle closer to the midplane and, hence, lead to higher dust number densities. The last square root term in Eq. 27 accounts for this effect.

We assume to be in a nearly non-turbulent region in the midplane of the disk, the so-called dead zone. Due to the high dust opacity in the midplane the ionization degree in this region is too low for the magneto rotational instability to operate (Balbus and Hawley 1991; Reyes-Ruiz 2001). However, there are other sources for turbulence, such as Kelvin Helmholtz instability (Weidenschilling 1979; Johansen et al. 2006), baroclinic instabilities (Klahr 2004; Petersen et al. 2007), and possibly free charges mixed to the interior of the disk from the upper layers leading to a slight coupling of the midplane gas to the magnetic fields (Turner et al. 2007). Therefore, we assume a low, but non-zero turbulent α -value of $\alpha = 10^{-5}$ (Cuzzi and Weidenschilling 2006). This low turbulent α -value influences the number densities of the dust as well as the relative velocities of solid particles in the disk (Ormel and Cuzzi 2007).

We identify three solar nebula models which

significantly spread the space of parameters in surface density. The first model is the minimum mass solar nebula (MMSN) model as calculated by Hayashi (1981) and Weidenschilling (1977). We adopt a second model based on recent interferometric millimeter observation of disks in the Taurus-Auriga and Ophiuchus-Scorpius star formation regions (Andrews and Williams 2007). These observations suggest much flatter surface density distributions than in the MMSN model. Finally, we consider a revised MMSN model which accounts for planetary migration in the early solar system (Desch 2007). In this new MMSN model, most of the mass is in the inner parts of the disk which leads to very high surface densities of several 10^4 g cm^{-2} , raising the question of gravitational instability. The surface densities at 1 AU and the power law indices δ of each disk model are given in Table 2. From these surface densities we can calculate the number density of aggregates (Eq. 27), also given in Table 2. For this calculation and also further on we use $T_0 = 280 \text{ K}$, $\epsilon = 0.5$, $M_\star = M_\odot$, and $\rho_d = 300 \text{ kg m}^{-3}$.

Different surface densities lead to different relative particle velocities in the protostellar disk. Figure 8 shows the relative velocities in the midplane of the disk at 1 AU for all three models. For calculating these velocities, we followed Brauer et al. (2008) and included Brownian motion, relative radial drift velocities, and relative velocities caused by turbulent gas motion as calculated by Ormel and Cuzzi (2007). We remark that these relative velocities may differ from earlier works due to the fact that we adopt more recent calculations of relative particle velocities in turbulence (Ormel and Cuzzi 2007), and because the solid particle density used here is only 300 kg m^{-3} accounting for porous particle growth.

To deduce the mean collision velocities of two nearly equal sized aggregates with radius R , we calculate relative velocities in the interval $[\frac{2}{3}R, \frac{4}{3}R]$, accounting for a not perfectly sharp size distribution, and take the mean relative velocity in this interval. Thus, collision velocity, number density (Eq. 27) and cross section yield the collision timescale τ_c for different models. We also scale the size of the aggregate (cf. section 4.1) so that we get a mean relative velocity of 0.2 m s^{-1} . For these sizes and velocities, we get collision timescales of less than a year. After the

time $\tau_c \cdot \nu$, the aggregates are significantly compacted and all these times are short in terms of planet formation.

4.3. Consequences for Further Protoplanetary Growth

We address three important consequences of the results of this work: *(i)* The aggregates are compacted and therefore change their surface-to-mass ratio. This has consequences for their coupling to the gas and their relative velocities. *(ii)* The compacted aggregate possesses macroscopic parameters like tensile strength, compressive strength and shear strength different to the strengths of the non-compacted aggregate. *(iii)* The finding of unexpected fragmentation requires a review of the fragmentation threshold.

(i) The friction time, the time in which a protoplanetary dust aggregate is coupled to the surrounding rarified gas, is in the free molecular flow regime defined as (Epstein 1924)

$$\tau_F = \frac{m}{\sigma_a} \frac{1}{\rho_g \bar{v}}, \quad (28)$$

where ρ_g and \bar{v} are the mass density and the mean thermal velocity of the gas. m and σ_a are properties of the dust aggregate, namely, its mass and its geometrical cross section $\sigma_a = \pi R^2$. In section 3.2 we found that the aggregate volume decreases by a factor of two within 1000 collisions without changing its mass, which increases its friction time by a factor of 1.6. The friction time determines the aggregate's velocity relative to the nebular gas and, thus, relative to other aggregates (Weidenschilling and Cuzzi 1993). As the size of the aggregate decreases from the compaction, its relative velocity would be that of an uncompacted aggregate with twice its diameter.

(ii) The macroscopic material parameters are clearly connected to the coordination number (number of contacts per dust grain) and thus to the volume filling factor. The compressive strength curve $\phi(p)$ (Blum and Schräpler 2004; Güttler et al. 2009, paper I) gives the relation for the compressive strength as a function of the filling factor. Blum and Schräpler (2004) measured the tensile strength for differently-compressed dust aggregates and found an increasing tensile strength, closely linear to the coordination number. The

shear strength (so far not measured for dust aggregates) is also believed to be depending on the filling factor (Sirono 2004; Schäfer et al. 2007; Güttler et al. 2009). Güttler et al. (2009) perform Smooth Particle Hydrodynamics simulations using macroscopic material parameters to develop a collision model for protoplanetary dust aggregates. Sirono (2004) found the occurrence of fragmentation to be depending on the ratio between tensile strength and compressive strength. As the compressive strength is much more sensitive to compaction than the tensile strength (Blum and Schräpler 2004), the compaction will clearly have an influence on the fragmentation threshold which is qualitatively shifted to smaller velocities.

(iii) The occurrence of fragmentation is rather surprising. Earlier experiments (Blum and Münch 1993, paper II) show fragmentation for velocities $\gtrsim 1 \text{ m s}^{-1}$, which is well above the maximum velocity of the experiments presented here (0.3 m s^{-1}). One possible explanation is a decreased fragmentation threshold due to the change of macroscopic parameters (see (ii)). However, Blum and Münch (1993) performed experiments with intermediate porosities ($\phi = 0.26$), still with a different material (ZrSiO_4), and found the same threshold. Explanations based on cracking and cumulative damage of the aggregate in multiple collisions are thinkable to reduce the aggregate strength but this – although of major importance – remains open for further investigation. A second possibility is a low but non-zero fragmentation probability, which would clearly be depending on velocity and material parameters, and has a finite value $P_{\text{frag}} = 1.8 \cdot 10^{-4}$ per collision for $v \approx 0.2 \text{ m s}^{-1}$. Although this probability disregards the history of the aggregate, it is so far the only possible treatment of the breakup in multiple collisions.

Acknowledgement

We thank the Deutsche Forschungsgemeinschaft for funding this work within the Forschergruppe 759 "The Formation of Planets: The Critical First Growth Phase" under grant Bl298/7-1.

REFERENCES

Andrews, S. M. and Williams, J. P. (2007). High-Resolution Submillimeter Constraints on Circumstellar Disk Structure. *ApJ*, 659:705–728.

- Balbus, S. A. and Hawley, J. F. (1991). A powerful local shear instability in weakly magnetized disks. I - Linear analysis. II - Nonlinear evolution. *ApJ*, 376:214–233.
- Blum, J. and Münch, M. (1993). Experimental investigations on aggregate-aggregate collisions in the early solar nebula. *Icarus*, 106:151.
- Blum, J. and Schräpler, R. (2004). Structure and Mechanical Properties of High-Porosity Macroscopic Agglomerates Formed by Random Ballistic Deposition. *Phys. Rev. Lett.*, 93(11):115503.
- Blum, J., Schräpler, R., Davidsson, B. J. R., and Trigo-Rodríguez, J. M. (2006). The Physics of Protoplanetary Dust Agglomerates. I. Mechanical Properties and Relations to Primitive Bodies in the Solar System. *ApJ*, 652:1768–1781.
- Blum, J. and Wurm, G. (2000). Experiments on Sticking, Restructuring, and Fragmentation of Preplanetary Dust Aggregates. *Icarus*, 143:138–146.
- Blum, J., Wurm, G., Kempf, S., Poppe, T., Klahr, H., Kozasa, T., Rott, M., Henning, T., Dorschner, J., Schräpler, R., Keller, H. U., Markiewicz, W. J., Mann, I., Gustafson, B. A., Giovane, F., Neuhaus, D., Feghtig, H., Grün, E., Feuerbacher, B., Kochan, H., Ratke, L., El Goresy, A., Morfill, G., Weidenschilling, S. J., Schwehm, G., Metzler, K., and Ip, W.-H. (2000). Growth and Form of Planetary Seedlings: Results from a Microgravity Aggregation Experiment. *Phys. Rev. Lett.*, 85:2426–2429.
- Brauer, F., Dullemond, C. P., and Henning, T. (2008). Coagulation, fragmentation and radial motion of solid particles in protoplanetary disks. *A&A*, 480:859–877.
- Brauer, F., Dullemond, C. P., Johansen, A., Henning, T., Klahr, H., and Natta, A. (2007). Survival of the mm-cm size grain population observed in protoplanetary disks. *A&A*, 469:1169–1182.
- Cuzzi, J. N. and Weidenschilling, S. J. (2006). *Particle-Gas Dynamics and Primary Accretion*, pages 353–381. Meteorites and the Early Solar System II.
- Desch, S. J. (2007). Mass Distribution and Planet Formation in the Solar Nebula. *ApJ*, 671:878–893.
- Dintwa, E., Tijskens, E., and Ramon, H. (2008). On the accuracy of the Hertz model to describe the normal contact of soft elastic spheres. *Granular Matter*, 10(3):209–221.
- Dominik, C. and Tielens, A. G. G. M. (1997). The Physics of Dust Coagulation and the Structure of Dust Aggregates in Space. *ApJ*, 480:647.
- Dubrulle, B., Morfill, G., and Sterzik, M. (1995). The dust subdisk in the protoplanetary nebula. *Icarus*, 114:237–246.
- Epstein, P. S. (1924). On the resistance experienced by spheres in their motion through gases. *Phys. Rev. Lett.*, 23(6):710–733.
- Güttler, C., Krause, M., Geretshausen, R., Speith, R., and Blum, J. (2009). Towards a Dynamical Collision Model of Highly Porous Dust Aggregates. In *Powders & Grains 2009 Conference Proceedings*. submitted.
- Hayashi, C. (1981). General Discussions - Fundamental Problems in the Theory of Stellar Pulsation. In *Fundamental Problems in the Theory of Stellar Evolution*, volume 93 of *IAU Symposium*, pages 339–342. D. Reidel Publishing Co.

- Heißelmann, D., Fraser, H., and Blum, J. (2007). Experimental Studies on the Aggregation Properties of Ice and Dust in Planet-Forming Regions. In *Proceedings of the 58th International Astronautical Congress 2007*. IAC-07-A2.1.02.
- Hertz, H. (1881). Über die Berührung fester elastischer Körper. *Journal für die reine und angewandte Mathematik*, 92:156–171.
- Johansen, A., Henning, T., and Klahr, H. (2006). Dust Sedimentation and Self-sustained Kelvin-Helmholtz Turbulence in Protoplanetary Disk Midplanes. *ApJ*, 643:1219–1232.
- Klahr, H. (2004). The Global Baroclinic Instability in Accretion Disks. II. Local Linear Analysis. *ApJ*, 606:1070–1082.
- Krause, M. and Blum, J. (2004). Growth and Form of Planetary Seedlings: Results from a Sounding Rocket Microgravity Aggregation Experiment. *Phys. Rev. Lett.*, 93(2):021103.
- Langkowski, D., Teiser, J., and Blum, J. (2008). The Physics of Protoplanetary Dust Agglomerates. II. Low-Velocity Collision Properties. *ApJ*, 675:764–776.
- Ormel, C. W. and Cuzzi, J. N. (2007). Closed-form expressions for particle relative velocities induced by turbulence. *A&A*, 466:413–420.
- Paszun, D. and Dominik, C. (2008). Numerical determination of the material properties of porous dust cakes. *A&A*, 484:859–868.
- Petersen, M. R., Julien, K., and Stewart, G. R. (2007). Baroclinic Vorticity Production in Protoplanetary Disks. I. Vortex Formation. *ApJ*, 658:1236–1251.
- Reyes-Ruiz, M. (2001). The Magnetorotational Instability across the Dead Zone of Protoplanetary Disks. *ApJ*, 547:465–474.
- Schäfer, C., Speith, R., and Kley, W. (2007). Collisions between equal-sized ice grain agglomerates. *A&A*, 470:733–739.
- Sirono, S.-I. (2004). Conditions for collisional growth of a grain aggregate. *Icarus*, 167:431–452.
- Turner, N. J., Sano, T., and Dziourkevitch, N. (2007). Turbulent Mixing and the Dead Zone in Protostellar Disks. *ApJ*, 659:729–737.
- Weidenschilling, S. J. (1977). The distribution of mass in the planetary system and solar nebula. *Ap&SS*, 51:153–158.
- Weidenschilling, S. J. (1979). Self-Induced Turbulence and the Onset of Gravitational Instability in a Dust Layer. *Bulletin of the American Astronomical Society*, 11:552.
- Weidenschilling, S. J. and Cuzzi, J. N. (1993). Formation of planetesimals in the solar nebula. In Levy, E. H. and Lunine, J. I., editors, *Protostars and Planets III*, pages 1031–1060.

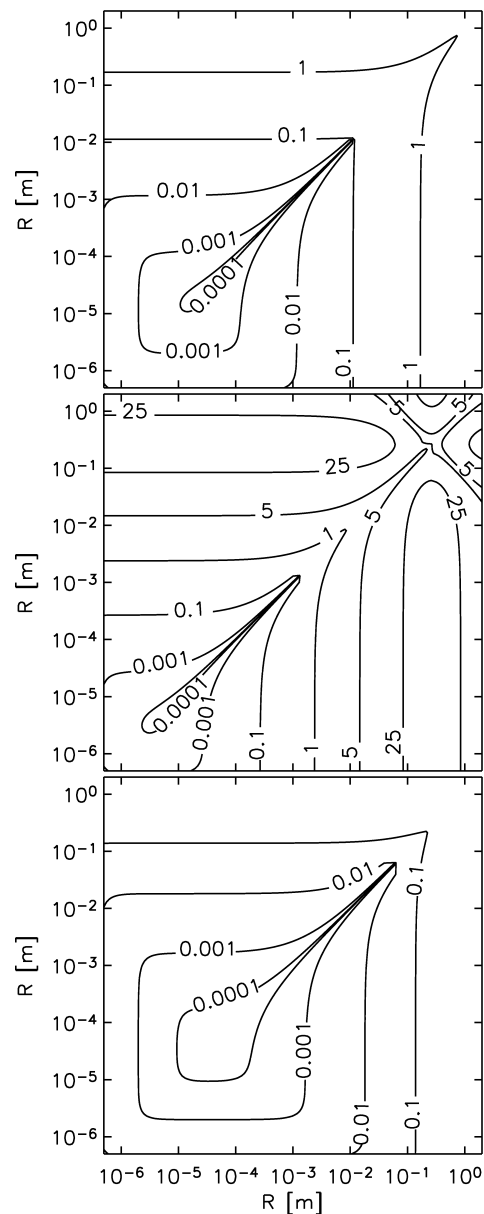


Fig. 8.— Relative velocities of dust aggregates in the protoplanetary disk midplane at 1 AU for different nebula models. Top to bottom Weidenschilling (1977), Andrews and Williams (2007), Desch (2007). The contour lines indicate velocities in m s^{-1} . The turbulence value is $\alpha = 10^{-5}$ (dead zone), and, accounting for porosity, the bulk density of the aggregates is 300 kg m^{-3} . The applied values for the surface density can be found in Table 2.